Journal of Engineering Science and Technology
Vol. 14, No. 4 (2019) 1820 - 1834

SIMULATION OF DISPLACEMENT DAMAGE CROSS SECTION OF CUPROUS OXIDE/ZINC OXIDE (Cu_2O/ZnO) BASED HETEROJUNCTION DEVICE

FUEI PIEN CHEE[1,*], MIVOLIL DUINONG[1], ABDUL ISMAIL ABDUL RANI[2], JACKSON HIAN WUI CHANG[3], AFISHAH ALIAS[4], SAAFIE SALLEH[1]

[1]Physics with Electronic Programme, Faculty of Science and Natural Resources, University Malaysia Sabah, Jalan UMS, 88400, Kota Kinabalu, Sabah, Malaysia
[2]Electrical and Electronics Engineering, Faculty of Engineering, University Malaysia Sabah, Jalan UMS, Kota Kinabalu, Sabah, Malaysia
[3]Preperatory Center for Science and Technology, University Malaysia Sabah, Jalan UMS, Kota Kinabalu, Sabah, Malaysia
[4]Department of Physics and Chemistry, Faculty of Applied Science and Technology, University Tun Hussein Onn Malaysia, 86400 Parit Raja, Johor, Malaysia
*Corresponding author: fpchee06@ums.edu.my

Abstract

In space, semiconductor devices are vulnerable to the various effect of a high energy level of radiation, causing Single Event Upsets (SEU), damaging or altering the lattice structure of the semiconductor device. The effect of energy level exposure and angle of trajectory on semiconductor device had received very little attention. In this research, the simulated sample is cuprous oxide/zinc oxide (Cu_2O/ZnO) based Heterojunction Device. The device was initially characterized using the General-Purpose Photovoltaic Device Model (GPVDM) simulation to obtain the current-voltage (IV) and current density-voltage (JV). The radiation damage was then modelled using cascade simulation on the effect of elastic and inelastic scattering by Cobalt-60 (^{60}Co) ions using Stopping and Range of Ions in Matter (SRIM-TRIM) simulation. GPVDM simulation shows, the recombination rate of hole and electrons at V_{oc} is obtained to be $3.985e^{-35}$ $m^{-3}s^{-1}$. SRIM-TRIM simulation shows that at 1.5 MeV particle radiation energy, it was found that the stopping range is about 1.07 μm and at a maximum energy of 10 MeV, the stopping range is about 4.08 μm. At $E_{Co} = 1500\,keV$, $E_{Co} = 5000\,keV$ and $E_{Co} = 10000\,keV$, the total ionization is 1173.8 keV/ Ion 4267 keV/Ion and 9550.8 keV/Ion at an ion angle trajectory of 60°. This paper highlights the roles of energy of the Primary Knock-on Atom (PKA) and the response of device to ion collision cascade at different irradiation angle.

Keywords: Cobalt-60, Cuprous oxide, GPVDM, Ionizing radiation, SRIM-TRIM, Zinc oxide.

1. Introduction

In the current age the application of Zinc Oxide (ZnO) semiconductor has become a prominent semiconductor material in fabrication where it has wide bandgap of II-VI semiconductor group (~3.3-3.4 eV), a high electron mobility, easily fabricated under low temperature [1], an efficient photon emission, can be easily n-doped, higher mobility than Silicon-based thin film transistor (SiTFTs) for the same degree of crystallinity, low resistance, high transparency, high translucency (>80%) and high conductivity, low cost and non-toxicity [2]. These advantages of ZnO could greatly overcome the flaws and replace the use of conventional SiTFTs [3]. A number of diverse methods had been used to fabricate ZnO channel layer including Radio Frequency (RF) sputtering [1], Metal Organic Chemical Vapour Deposition (MOCVD) [4] and Pulse Laser Deposition (PLD) [5].

In terms of metal oxides research, ZnO and Cu_2O are considered to be one of the most notable materials due to its affordability and compatibility in a variety of electrical devices. In addition, it has riveting optical and I-V (current-voltage) properties. Research on p-type Cu_2O and n-type ZnO based thin film heterojunction has received attention due to its deposition flexibility using various known methods such as magnetron sputtering [6], Chemical Vapour Deposition (CVD) [7], Molecular Beam Epitaxy (MBE) [8] and electrochemical deposition [9].

At present, space application of oxide-based semiconductor material is starting to gain attention where its superiority over amorphous silicon-based material is greatly noticeable [2]. When ZnO based films were irradiated with Co-60 it shows degradation in the turn-on voltage and appearance of low-frequency noise [8, 10]. The electron mobility is found to benefit from the exposure and shows a significant increment. The changes in the electrical properties in the films are induced by the irradiation are attributed to the combined effects of interface states creation and electron-hole pair generation in the insulating layer [10]. The necessity of research on the durability of zinc oxide towards radiation exposure is vital as previous research reveals that the resistance of ZnO towards radiation effects were better than most conventional semiconductor materials and emerging transistor technologies [11].

Based on research conducted by Nastasi et al. [12], it was stated that bombardment of a crystal with energetic (kilo-electron volts to mega-electron-volts) heavy ion produces regions of lattice disorder. This dislocation highly depends on ion species, temperature, energy, total dose and channelling effects. In addition, the parameters that give effect to the formation of radiation damage are the ion mass, ion species, the target temperature during irradiation, total dose, ion's energy and the ion's flux (number of ions per unit area) [13, 14]. The bombardment of the solid with ions in the electron-volt (eV) to mega-electron-volt (MeV) energy range might affect the physical, mechanical, electrical, optical, magnetic and superconducting properties [13].

In a related study conducted by Chee et al. [13], simulation on GaAs with an iron incident energy level ranging from 100 keV to 3 MeV was carried out using SRIM The findings of this research reports that exposure of high energy photon irradiation causes degradation to the electrical parameters due to displacement damage. In another similar study conducted by Movla et al. [15], simulation on GaAs with a thickness of 10 μm based solar cells were carried out using SRIM 2013 package. Based on the previous report, the effects of the 1 MeV of α particle

radiation on GaAs simulated using SRIM-TRIM shows a stopping range of 3.5 μm and a large part of the damage occurs in the silver (Ag) metal contact. Simulation of damage induced considers only on a single trajectory. Both studies simulate only for a single trajectory without considering the simulation damage caused by alteration on the irradiation angle.

The aim of this paper is to highlight the roles of the energy of the Primary Knock-on Atom (PKA) and the response of the device to ion collision cascade at different irradiation angle.

2. Research Approach

In this research, a simulation on a heterojunction device of ITO (Indium Tin Oxide, which is a transparent electrode): ZnO/Cu_2O (active material) /Al (electrode) was established by using a General-Purpose Photovoltaic Device Model (GPVDM) simulator at selected thickness of Zinc Oxide and Cuprous Oxide to obtain the I-V characteristic of the ZnO/Cu_2O based heterojunction device. Once the early characterization on the I-V characterization was obtained, a simulation of damage induced in ZnO/Cu_2O based heterojunction was carried out using Stopping and Range of Ions in Matter (SRIM) simulation package.

2.1. GPVDM

GPVDM software is developed for the simulation of Organic Solar Heterojunction Device (OPV), α-Si Solar Heterojunction device, OFET, Organic LED, Perovskite Solar Heterojunction device and Polycrystalline Silicon model. This model is applied in this study for the simulation of electrical and optical properties. I-V and J-V graph are plotted and obtain from the simulation results to reveal the pattern of the electron density when a voltage is applied to the stimulated device. Eq. (1) and Eq. (2) are applied to generate the I-V and J-V curve. The electrical simulation only covers for the active layer of the device as the main reaction occurs on the active layer of a device.

$$I = I_{\circ}\,(e^{\frac{qV}{kT}} - 1) \tag{1}$$

$$j_{external} = i_{ideal} + \frac{V_{applied}}{R_{shunt}} \tag{2}$$

2.2. SRIM-TRIM

SRIM is a software package concerning the Stopping and Range of Ions in Matter [16]. It has been continuously upgraded since its introduction in 1985 [17]. SRIM uses the Core and Bond (CAB) approach to simulate the high energy atomic collision [18].

The core stops would simply follow Bragg's rule for the atoms of the compound, where SRIM linearly add the stopping from each of the atoms in the compounds [18]. TRIM (Transport of Ions in the Matter) accepts up to eight complex targets from various materials [16]. This simulation gives the calculation results for the 3D spread of ions, damage of the target, sputtering, ionization and phonon production. The total displacement atoms in the lattice are a sum of a number of vacancies and replacement collisions [16]. When a recoil atom stops and is not a replacement atom, then it becomes an interstitial.

In this research, the incident atom ^{60}Co has an atomic number Co_{27} and assumed with energy of $E=E_{Co\text{-}60}$. It has a collision within the target with Zn of atomic number Zn_{30}. After the collision, the incident ion with energy of 1MeV and the struck ZnO atom has energy E_2= 629 keV/Ion. Previously specified for the target (ZnO) are energies E_d, the displacement energy at 52 eV [19], E_b, the binding energy at 60 meV [20] of a lattice ZnO with to its site, and E_f, the final energy of the moving atom of ZnO at 10 MeV below, which it is considered to be stopped. Table 1 shows the parameters, which is utilized in this simulation.

Table 1. Parameters for simulation [19, 20].

No.	Parameters	Parameter's value	Symbols
1.	Incident Ion energy of Cobalt-60	1 MeV	E_1
2.	Energy of struck ZnO	629 keV/Ion	E_2
3.	Displacement energy of Zinc Oxide	52 eV	E_d
4.	Average surface binding energy of ZnO	60 meV	E_b
5.	Atomic mass of Co-60	27	Z_1
6	Atomic mass of ZnO	38	Z_2

- A displacement occurs if the energy that strikes the atom ZnO, E_2 > the average surface binding energy of ZnO, E_d. [16].
- A vacancy occurs if both the incident Ion energy of Cobalt-60, E_1 > the average surface binding energy of ZnO, E_d and if the energy that strikes the atom ZnO, E_2 > the average surface binding energy of ZnO, E_d (both atoms have enough energy to leave the site). Both atoms then become moving atoms of the cascade. The energy that strikes the atom ZnO, E_2 is reduced by the average surface binding energy of ZnO, E_b before it has another collision [16].
- If the energy that strikes the atom ZnO, E_2 < the average surface binding energy of ZnO, E_b, the struck atoms ZnO does not have enough energy and it will vibrate back to its original site releasing the energy intended to strike the surface of ZnO, E_2 as phonons [16].
- If the incident of ion energy of Cobalt-60, E_1 < the average surface binding energy of ZnO, E_d and the energy that strikes the atom ZnO, E_2 > the average surface binding energy of ZnO, E_d and the atomic number of $Z_1 = Z_2$, then the incoming atom will remain at the site and the collision is called a replacement collision with E_1 released as phonons [16].

Therefore, when the incident Ion energy of Cobalt-60, E_1 < the average surface binding energy of ZnO, E_d and the energy that strikes the atom ZnO, E_2 > the average surface binding energy of ZnO, E_d and $Z_1 = Z_2$, then the incoming atom will remain at the site and the collision is called a replacement collision with E_1 released as phonons [16].

Finally, if the incident Ion energy of Cobalt-60, E_1 < the average surface binding energy of ZnO, E_d and the energy that strikes the atom ZnO, E_2 < the average surface binding energy of ZnO, E_d, then Z_1 becomes an interstitial and $E_1 + E_2$ is released as photons. If the target has several different elements in it, the same as the proposed heterojunction device and each has different displacement energy, E_d will change for each atom of the cascade hitting different target atoms.

3. Results and Discussion

3.1. GPVDM simulation

In this simulation, the thickness is the main parameter as the thickness of the active layer is important in determining the efficiency of the device. The thickness of ZnO active layer is 300 nm same with the p-type material of Cu_2O while the thickness of ITO and Al is 180 nm and 200 nm [21, 22]. The numerical modelling reveals that the thickness of Cu_2O and ZnO affect the electrical properties.

To operate this simulation, different types of materials can be chosen in the materials directory [23]. In this case, ZnO and Cu_2O is chose to be the active layer of the device. Before running the simulation, the configuration of the device is confirmed to be set up along with the required thickness, the general simulation parameter is set and shown in Table 2.

Table 2. Default parameter value used in GPVDM simulation [24].

No.	Parameters	Parameter's value	Units
1.	Electron trap density	1×10^{15}	m^{-3} eV^{-1}
2.	Hole trap density	1×10^{15}	m^{-3} eV^{-1}
3.	Electron mobility	1×10^{-5}	M^2 V^{-1} s^{-1}
4.	Hole mobility	1×10^{-5}	M^2 V^{-1} s^{-1}
5.	Number of traps	20	-
6.	Free electron to trapped hole	1×10^{-25}	m^{-2}
7.	Trapped electron to free hole	1×10^{-25}	m^{-2}
8.	Trap hole to free electron	1×10^{-25}	m^{-2}
9.	Free hole to trapped hole	1×10^{-25}	m^{-2}

Figure 1 shows the *J-V* characteristic of the simulated device. The value of current density increases as the applied voltage increase in the simulation as the movement between hole and electron are rapidly carrying the charge passing through the interface. The graph does not pass zero point due to the charging effect of the simulated device [24]. Recombination rate of hole and electrons at V_{oc} is $3.985e^{-35}$ $m^{-3}s^{-1}$.

The number of minority carrier accumulated at the junction edge is controlling the rate of recombination through the movement of the carrier and the speed of the recombination process. Consequently, a higher recombination rate will have increased the forward bias diffusion current into the system thus, reducing the open circuit voltage. Based on the analysis, it shows that the threshold voltage for ZnO *p-n* junction is ≤ 1 V. The value of threshold voltage obtain is lower compared to other material such as ZnSe and GaN, which they have threshold voltage in the range of 1.2 V - 1.4 V and 2.6 V - 3 V, which is in agreement to past researched [25].

The value of threshold voltage is important because it determines the device performance for a lifetime. Lower threshold voltage ensures ZnO based device operating for a longer period of time without a serious ohmic heating problem at the contact of the device [26]. Referring to Figs. 2 and 3, the distribution of photon is at the highest at the thickness of 500 nm to 600 nm from the sputtered heterojunction, which corresponds to the maximum energy dissipated in the device is (3eV). The crystalline structure of sputtered material controlled the distribution of the photon as higher crystallize properties will increase the transfer of charge in the active layer thus, increasing the efficiencies of the fabricated device [27, 28].

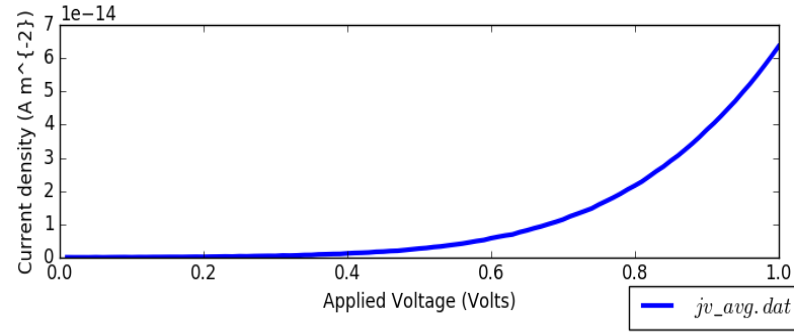

Fig. 1. *J-V* characteristic of simulated device.

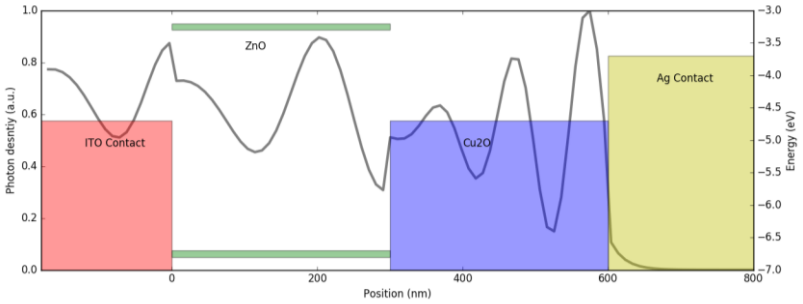

Fig. 2. Distribution of photon density in device.

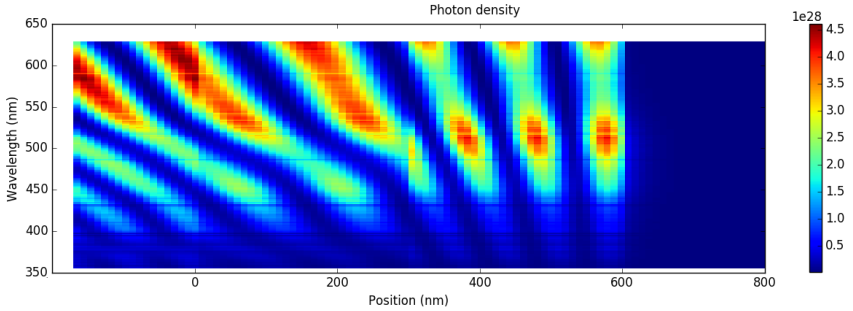

Fig. 3. Distribution of photon density based on visible light wavelength.

3.2. SRIM-TIM simulation

Once the preliminary characterization was done using the GPVDM simulation, the study was proceeded using SRIM to simulate the high energy atomic collision of Cobalt-60 ion ^{60}Co. In this simulation, Cobalt-60 was used as the incident ion, a radioactive element that simulates the emission of γ-rays. Cobalt-60 is produced by neutron bombardment of stable cobalt in a nuclear reactor. γ-rays are considered to be photons, which are electromagnetic radiation that can interact with the crystal structure. The interaction that occurs in the crystal structure is similar to a photoelectric effect that undergoes inside the semiconductor device, which causes

the bond of valence electron to be emitted into the conduction band across the band gap energy, E_g leaving behind a hole. The after effect leads to the creation of a free electron-hole pair. At a greater energy level, Compton scattering occurs causing the incident photon to be deflected from its original path due to the interaction with an electron that is free or relatively bound to an atom [28]. In this interaction, the photon loses energy as part of the photon energy is transferred to the electron, which in turn yields the emission of a secondary lower energy photon.

To operate the simulation of this software, the simulation on the Stopping and Range of the Ion Matter (SRIM) must be performed first to determine the maximum projection range of the energy on the semiconductor device used. The first step in operating the SRIM software is by selecting the incident ion-atom ^{60}Co followed by the range of ion emission energy ranging from 0.1 to 10 MeV.

From the simulation, data tabulated is as shown in Fig. 4. The Cobalt-60 stopping energy has an exponential rate and it is found that in 1.5 MeV radiation energy, the stopping range of ^{60}Co ion in the device is about 1.07 μm. The thickness of the semiconductor device simulated in this research has an overall thickness of 1.08 μm, the projection range that is admissible is at 1.07 μm with an energy of 1.5 MeV. In addition, the maximum projection range of the ion energy at 10 MeV has a stopping range of 4.08 μm.

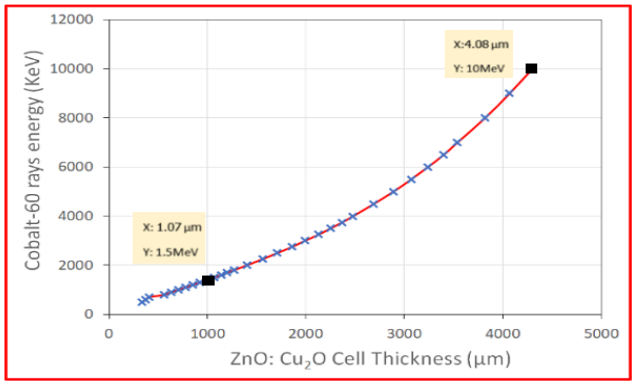

Fig. 4. Stopping range of Cobalt-60 in ZnO/Cu$_2$O based heterojunction device.

3.3. Effects of incident energy of Cobalt-60 (^{60}Co) ion

Upon the completion of the SRIM simulation, the simulation was continued using the Transport of Ions in Matter (TRIM) simulation to calculate the interactions of energetic ions with the device being studied. In this research, simulation using detailed calculation with full damage cascades. The operation is furthered by selecting the ion data used, in this case, Cobalt-60 (^{60}Co). Once incident ion energy has been selected, the selection of the target layers is added, and the simulation is initiated. The first simulation that was carried out was on the effects of the energy level of incident ^{60}Co ion. A total of 9 different energy level was utilized at 500 keV, 600 keV, 700 keV, 800 keV, 900 keV, 1000 keV, 1500 keV, 5000 keV and 10000 keV. From the simulation, Fig. 5 shows that the higher the incident energy, the higher the degree of damage created in the device simulated. However, fluctuations can be

observed at an energy level of 5000 keV and 10000 keV. From Fig. 5, the significance of data changes can be observed at 1500 keV, 5000 keV and 10000 keV.

Figure 5 also compares the energy absorbed and the displacement of the target layer at a different energy level. It is shown that at a higher energy level of ^{60}Co ion, the higher the damage density on the target. However, it is observed at E_{Co} =5000 keV and $E_{Co} = 10000\ keV$ the damage density is lower. This is because if the thickness of the target material (1.07 μm) is relatively smaller compared to the projected range of the given energy, the energy loss in the target damage will be diminished. This is due to the fact that the incidence of ^{60}Co ions have less interaction with the incidence target. From the Fig. 5, it is observed that the displacement of ^{60}Co ions into the target increases with energy, where the energetic incident atom of ^{60}Co knocks on the lattice atom of the ZnO/Cu_2O target causing vacancies in the target.

As shown in the plotting, Fig. 5, highest ion distribution of ^{60}Co ion occurs at an incidence at 1500 keV. Ion distribution is the distribution of the ^{60}Co ion distributed into the ZnO/Cu_2O heterojunction device. Atoms are displaced by the incident ion knocking the atom off its lattice site causing lattice displacement either displaced by the incident ion of ^{60}Co or by the recoils of the other atoms within the ZnO/Cu_2O atom heterojunction device causing vacancies. The dispersed white dots in Fig. 6 indicates the distribution of ^{60}Co ion travelling through the target atoms resulting in lattice displacement. The other colours dispersion of dots and clusters, however, indicates the displacement of the targeted atom, which leads to the formation of vacancies of due to the recoils of the other atoms.

As illustrated in Fig. 6, the distribution plots at 1.5 MeV are dominated mostly due to recoiling atoms with a total vacancy of 12180 keV/Ion and a replacement collision of 393 keV/Ion. In comparison to $E_{Co} = 5000\ keV$ and $E_{Co} = 10000\ keV$, ionization induced by ^{60}Co ions are greater than the recoiling target atoms. At $E_{Co} = 5000\ keV$, the total vacancy form is 4075 keV/Ion and a replacement collision of 129. The reduction of vacancy formation of the ZnO/Cu_2O atom heterojunction device at $E_{Co} = 5000\ keV$ is due to the fact that, at a higher energy level, ionization induced by ^{60}Co ion are greater in comparison to the displacement of target atoms resulting to a lower vacancy but higher lattice displacement. At $E_{Co} = 10000\ keV$, the total vacancy form is 2201 keV/Ion with a replacement collision of 71. From the data obtained in Fig. 5, it can be concluded that, lower energy level leads to displacement of target atoms forming a vacancy while at higher energy levels, while at energy higher than 1.5 MeV, the damage induced is reduced due to less energy is deposited by the high impulse of ^{60}Co ion during the projection.

At lower incidence energy, energy deposition occurs mainly at the surface of the target, displacing a large amount of the lattice atoms from the surface thus, inducing a significant number of recoiling atoms. The recoiling of the other atoms within the target will then result in the formation of vacancy. In addition, recoiling atoms tend to be more active than ^{60}Co ions at a lower energy level where it has sufficient energy to experience ionization. Based on Figs. 5 and 7, the simulated data show that ionization of ^{60}Co Ion is proportional to the energy level. At $E_{Co} = 1500\ keV$, $E_{Co} = 5000\ keV$ and $E_{Co} = 10000\ keV$, the total ionization is, 943.7 keV/Ion, 4658.4 keV/Ion and 9767.6 keV/Ion respectively. It can be concluded that Ionization of ^{60}Co ion is dependent on the incident energy level, where a higher energy yields a higher ionization induced in the targeted device. At higher energy level however, ionization induced by ^{60}Co is greater as they move and travel faster

than the recoiling target atoms. This circumstance is due to the fact that at a higher energy level, the pair production process is most likely to occur when the incident energy of ^{60}Co ions goes higher, which leads to the formation of an electron and positron resulting to the domination of the ^{60}Co ionization in the target.

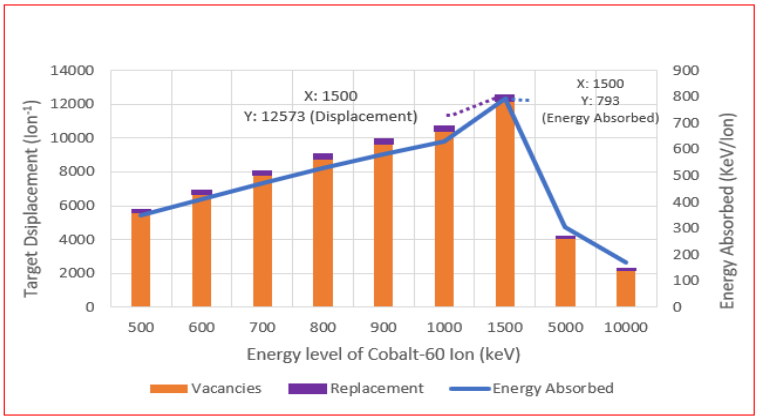

Fig. 5. Target displacement and energy absorbed of ZnO:Cu$_2$O heterojunction device at different incident energy level.

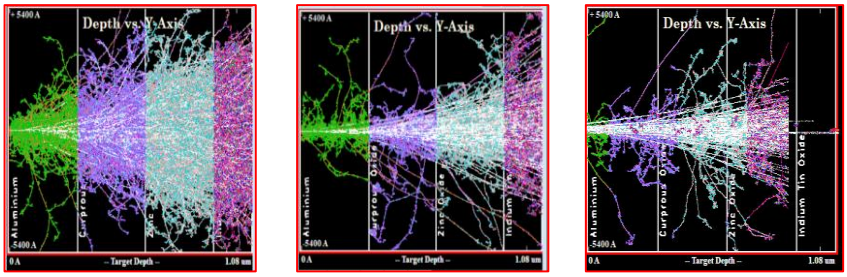

a) 500 keV. **b) 5000 keV.** **c) 10000 keV.**

Fig. 6. Plot of depth versus Y-axis at (a)$E_{Co} = 500\ KeV$, (b)$E_{Co} = 5000\ KeV$, (c) $E_{Co} = 10000\ KeV$ in ZnO: Cu$_2$O heterojunction device.

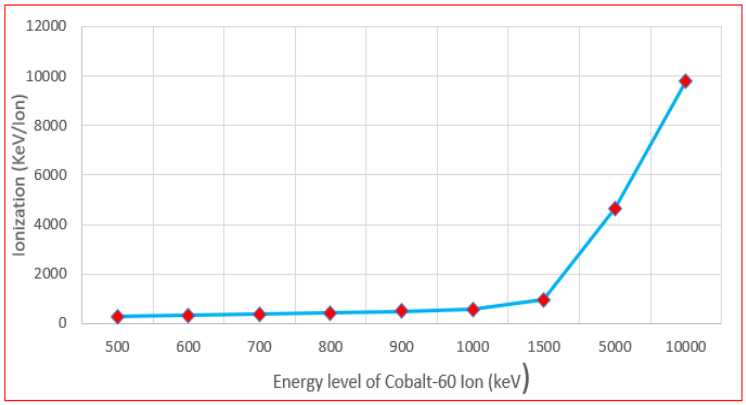

Fig. 7. Ionization of ^{60}Co against energy level.

3.4. Effects of ion angle trajectory of Cobalt-60 (^{60}Co) ion

From the previous section above, it was concluded that at a higher energy level of ^{60}Co ion, the higher the damage density on the target. This deduction is shown to be valid as long as the condition that the thickness of the target material is greater than the projected range of the given energy. In addition, it is also discovered that ionization is proportional to the increment of the energy level of the incidence ion. In this part of the simulation, the effects of different trajectory ion angle of ^{60}Co were carried out with 4 different angles of 0°, 30°, 60° and 90° at 500 keV, 600 keV, 700 keV, 800 keV, 900 keV, 1000 keV, 1500 keV, 5000 keV and 10000 keV respectively. Based on Figs. 8 to 10, it is shown that by increasing the ion angle trajectory of the incidence energy, the degree of damage created in the device simulated is smaller. However, it is shown that this occurrence does not apply at $E_{Co} = 5000\,keV$ and $E_{Co} = 10000\,keV$ at an angle ion trajectory of 60°. Based on Fig. 10, at an angle of 90° the trend of the slope is not similar for Figs. 8 and 9. This is due to the fact that at a greater angle of incident energy, ionization induced by ^{60}Co moves and travels only at a limited part of the target device thus, ignoring the factor of the maximum threshold of the overall thickness of the device (1.08 μm).

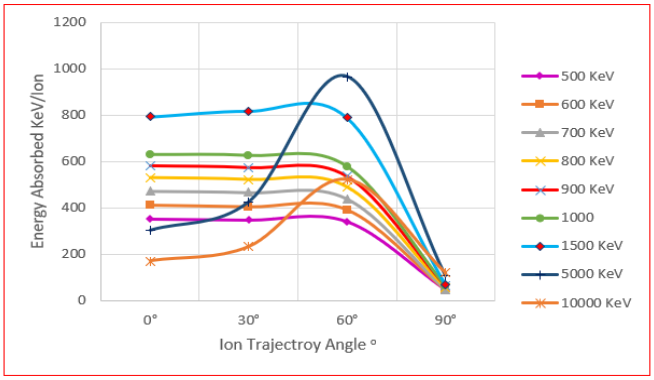

Fig. 8. Target displacement in ZnO/Cu$_2$O heterojunction device at multiple ion trajectory angles of 0°, 30°, 60°, 90° with different incident energy.

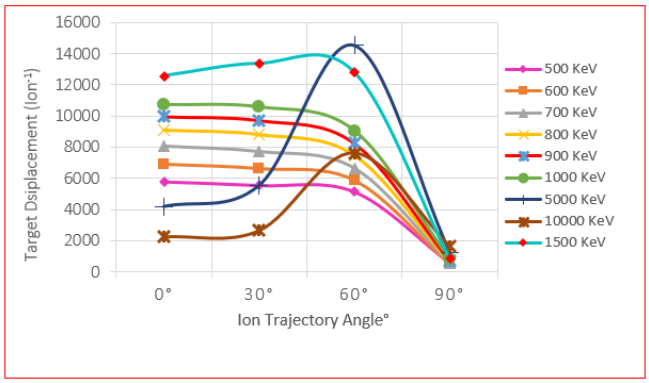

Fig. 9. Energy absorbed in ZnO/Cu$_2$O heterojunction device at multiple ion trajectory angles of 0°, 30°, 60°, 90° with different incident energy.

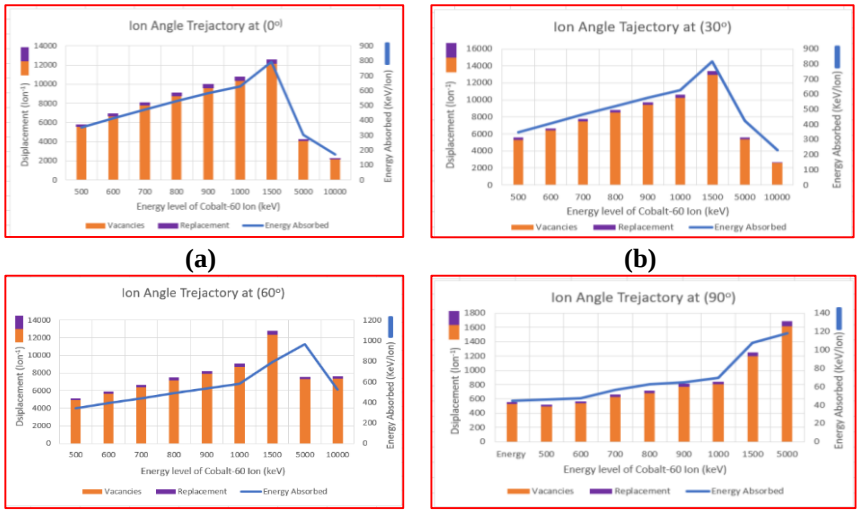

Fig. 10. Target displacement and energy absorbed of ZnO/Cu_2O heterojunction device at different incident energy level at multiple ions.

From the simulated result obtained in Fig. 11, the ion distribution plots of ^{60}Co at $E_{Co} = 5000\ keV$ are mostly dominated due to recoiling atoms (green colour line) in comparison to $E_{Co} = 10000\ keV$ where ionization induced (white colour line) by ^{60}Co ion are greater than the recoiling target atoms. At an angle trajectory of 0°,30° and 90° all 9-different energy level follows the trend of lower damage density with the increase of ion angle trajectory, except at an angle ion trajectory of 60°. This indicates that at a trajectory ion angle of 60°, energy levels at $E_{Co} = 5000\ keV$ and $E_{Co} = 10000\ keV$, has a lower projection range compared to the thickness of the target therefore, allowing ^{60}Co ion to have greater interaction with the incidence target.

Based on Figs. 8 and 9, it shows that greater damage is induced, with an exception for energies at $E_{Co} = 5000\ keV$ and $E_{Co} = 5000\ keV$ at an ion trajectory angle of 60°. This is due to the fact that by altering the angle of incidence, ionization induced by ^{60}Co moves and travels only at a limited part of the target device as shown in Fig. 11, where lattice displacement and vacancies only occurs at a limited region of the surface. At $E_{Co} = 1500\ keV$ $E_{Co} = 5000\ keV$ and $E_{Co} = 10000\ keV$, the total ionization is 1173.8 keV/Ion 4267 keV/Ion and 9550.8 keV/Ion at an ion angle trajectory of 60°. In comparison to the previous data obtained at the same energy with an angle of 0^0, ionization is lower for both, $E_{Co} = 5000\ keV$ and $E_{Co} = 10000\ keV$ with an ion angle trajectory of 60°. This is due to the fact that most of the ionization is a result from the recoiling atoms therefore, leading to a greater vacancy.

Based on Figs. 12 and 13, in comparison to Fig. 7, it is shown that by increasing the trajectory of the ion angle, ionization of ^{60}Co is higher. From the data obtained for both ion energy and trajectory angle, a perfect combination of p-n heterojunction device is yet to be discovered tested under harsh radiation environment. It is suggestible for future researchers on the simulation of SRIM-TRIM to make a physical comparison beforehand as external factors are not included in this simulation, where the said device is simulated under a perfect fixed environment without a physical data comparison.

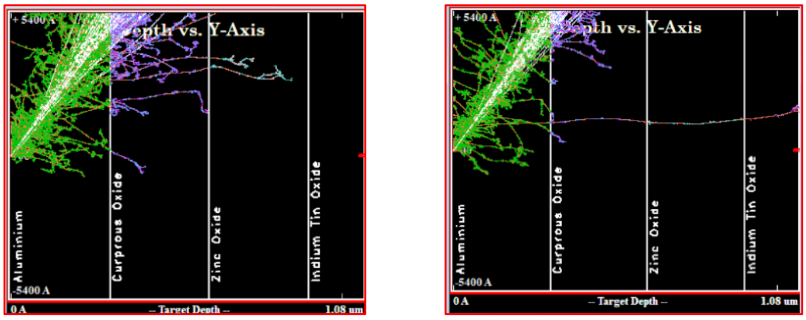

(a) 5000 keV. **(b) 10,000keV.**

Fig. 11. Plot of depth versus Y-axis at (a) E_{co}= 5000 keV, (b) 10000 keV in ZnO: Cu_2O heterojunction device with an ion trajectory angle of 60º.

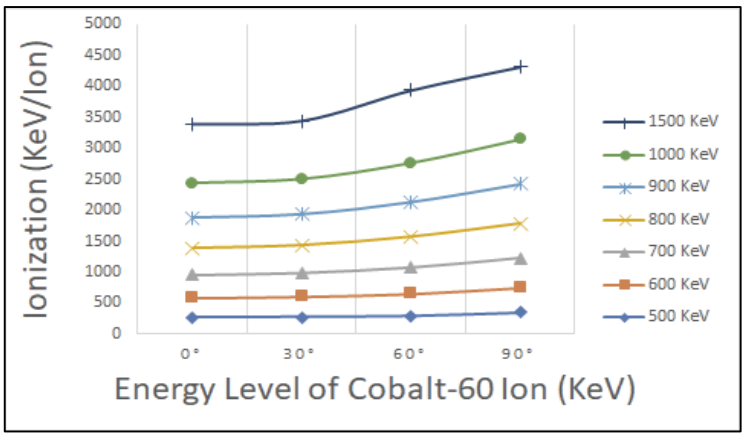

Fig. 12. Ionization of ^{60}Co at different energy level with Ion angle trajectory of 0°, 30°, 60°, 90º.

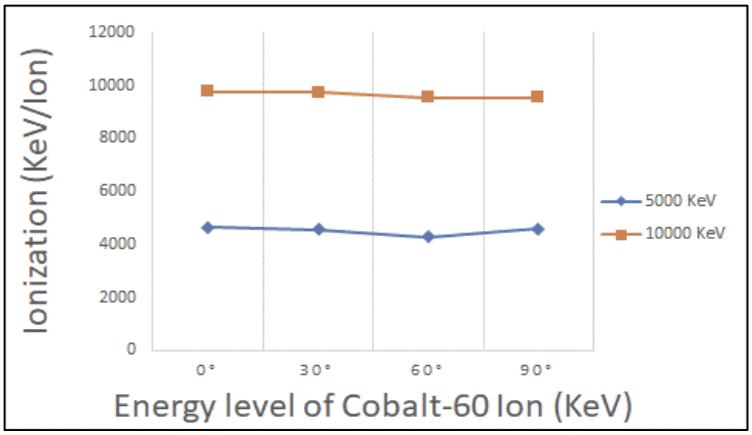

Fig. 13 Ionization of ^{60}Co at 5000 keV and 10000 keV energy level with ion angle trajectory of 0°, 30°, 60°, 90º.

4. Conclusion

In this paper, the effects of a different energy level of ^{60}Co ion radiation on the ZnO/Cu_2O heterojunction device have been investigated. An ideal I-V and J-V curve were obtained from the GPVDM based on the selected configuration of the heterojunction device. The value of open circuit voltage, V_{oc} is obtained by the simulation to be $3.985e^{-35}$ m^{-3} s^{-1}, showing the correlation between the recombination rate of the electron and forward bias diffusion current into the system. Besides that, it is found that the highest distribution of photons falls on the range of 500 nm to 600 nm thickness of the device and dissipated the maximum amount of energy of 3eV in the device.

To summarize it all, increasing the incidence ion energy will result to higher target damage with the condition that the projection range of the incidence ion energy is not greater than the overall thickness of the target, higher ionization of ^{60}Co ion while changing the incidence ion angle trajectory leads to a lower target damage with a condition that the energy level does not exceed greater than 1.5 MeV and ion trajectory must not be 60^o.

Acknowledgement

This research was supported by the Ministry of Higher Education Fundamental Research Grant Scheme (FRGS) 2016 under the project FRGS/1/2016/STG02/UMS/02/2 with the title "Investigation of Damage Mechanism of Zinc Oxide Thin Film Transistors (ZnO TFTs) due to neutron Radiation for Flexible Electronic in Space Application and University Malaysia University Malaysia Sabah Research Priority Area Scheme (SPBK) 2017 under the project number GUG0131-1/2017 with title Investigation of Ionizing Radiation Effects on Zinc Oxide Semiconductor Materials for Thin Film Transistors (TFT) Technology Application. The support from both parties is greatly acknowledged.

Nomenclatures

I	Anode current in Amps
I_o	Device saturation current
i_{ideal}	Ideal ccrrent
$j_{external}$	External current densities
k	Bolzmann's constant
q	Charge of electron
R_{shunt}	Shunt resistance
T	Temperature in Kelvin
V	Junction anode and cathode voltage
$V_{applied}$	Applied voltage to system

Abbreviations

GPVDM	General Purpose Photovoltaic Device Model
ITO	Indium Tin Oxide
SRIM	Stopping and Range of Ions in Matter

References

1. Hirao, T.; Furuta, M.; Hiramatsu, T.; Matsuda, T.; Li, C.; Furuta, H.; Hokari, H.; Yoshida, M.; Ishii, H.; and Kakegawa, M. (2008). Bottom-gate zinc oxide thin-film transistors (ZnO TFTs) for AM-LCDs. *IEEE Transactions on Electron Devices*, 55(11), 3136-3142.
2. Ozgur, U.; Hofstetter, D.; and Morkoc, H. (2010). ZnO devices and applications: A review of current status and future prospects. *Proceedings of the IEEE*, 98(7), 1255-1268.
3. Navamathavan, R.; Lim, J.-H.; Hwang, D.-K.; Kim, B.-H.; Oh, J.-Y.; Yang, J.-H.; Kim, H.-S.; and Park, S.-J. (2006). Thin-film transistors based on ZnO fabricated by using radio-frequency magnetron sputtering. *Journal of the Korean Physical Society*, 48(2), 271-274.
4. Remashan, K.; Choi, Y.S.; Park, S.J.; and Jang, J.H. (2012). Impact of near-stoichiometric silicon nitride gate insulator on the performance of MOCVD-grown ZnO thin-film transistors. *ECS Journal of Solid State Science and Technology*, 1(4), Q70-Q78.
5. Gupta, P.; Dutta, T.; Mal, S.; and Narayan, J. (2012). Controlled p-type to n-type conductivity transformation in NiO thin films by ultraviolet-laser irradiation. *Journal of Applied Physics*, 111(1), 013706-013706.7.
6. Fan, Z.; Wang, D.; Chang, P.-C.; Tseng, W.-Y.; and Lu, J.G. (2004). ZnO nanowire field-effect transistor and oxygen sensing property. *Applied Physics Letters*, 85(24), 5923-5925.
7. Stavale, F.; Pascua, L.; Nilius, N.; and Freund, H.J. (2013). Morphology and luminescence of ZnO films grown on a Au (111) support. *The Journal of Physical Chemistry C*, 117(20), 10552-10557.
8. Liu, Y.; Wu, W.-J.; En, Y.-F.; Wang, L.; Lei, Z.-F.; and Wang, X.-H. (2014). Total dose ionizing radiation effects in the indium-zinc oxide thin-film transistors. *IEEE Electron Device Letters*, 35(3), 369-371.
9. Ievskaya, Y.; Hoye, R.L.Z.; Sadhanala, A.; Musselman, K.P.; and MacManus-Driscoll, J.L. (2015). Fabrication of ZnO/Cu2O heterojunctions in atmospheric conditions: Improved interface quality and solar cell performance. *Solar Energy Materials and Solar Cells*, 135, 43-48.
10. Indluru, A.; Holbert, K.E.; and Alford, T.L. (2013). Gamma radiation effects on indium-zinc oxide thin-film transistors. *Thin Solid Films*, 539, 342-344.
11. Ramirez, J.I.; Li, Y.V.; Basantani, H.; and Jackson, T.N. (2013). Effects of gamma-ray irradiation and electrical stress on ZnO thin film transistors. *Proceedings of the 71st IEEE Annual Device Research Conference (DRC)*. Notre Damme, Indiana, United States of America, 171-172.
12. Nastasi, M.; Mayer, J.W.; and Hirvonen, J.K. (1996). *Ion-solid interactions: fundamentals and applications*. Cambridge, United Kingdom: Cambridge University Press.
13. Chee, F.P.; Amir, H.F.A.; and Salleh, S. (2011). Range distribution and electronic stopping power for Cobalt (Co) ions in Gallium Arsenide (GaAs) optoelectronic devices. *Proceedings of the 4th International Conference* on *Modeling, Simulation and Applied Optimization (ICMSAO)*. Kuala Lumpur, Malaysia, 1-5.

14. Wendler, E. (2009). Mechanisms of damage formation in semiconductors. *Nuclear Instruments and Methods in Physics Research Section B: Beam Interactions with Materials and Atoms*, 267(16), 2680-2689.
15. Movla, H.; Babazadeh, M.; and Sadreddini, S.V. (2016). Influence of α particle radiation on the structural and electronic properties of thin film GaAs solar cells: A simulation study. *Optik*, 127(8), 3844-3847.
16. Ziegler, J.F.; Ziegler, M.D.; and Biersack, J.P. (2008). SRIM: The stopping and range of ions in matter (2010). *Nuclear Instruments and Methods in Physics Research Section B: Beam Interactions with Materials and Atoms*, 268 (11-12), 1818-1823.
17. Andreo, P. (1991). Monte Carlo techniques in medical radiation physics. *Physics in Medicine and Biology*, 36(7), 861-920.
18. Sabin, J.R.; and Oddershede, J. (1987). Theoretical stopping cross sections of C□H, C□C and C=C bonds for swift protons. *Nuclear Instruments and Methods in Physics Research Section B: Beam Interactions with Materials and Atoms*, 27(2), 280-286.
19. Locker, D.R.; and Meese, J.M. (1972). Displacement thresholds in ZnO. *IEEE Transactions on Nuclear Science*, 19(6), 237-242.
20. Klingshirn, C.F.; Waag, A.; Hoffmann, A.; and Geurts, J. (2010). *Zinc oxide: From fundamental properties towards novel applications*. Heidelberg, Germany: Springer-Verlag Berlin Heidelberg.
21. Li, L.M.; Mani, A.M.; Shain, F.L.; Alias, A.; and Salleh, S. (2015). Effect of sputtering pressure on the structural and optical properties of ZnO films deposited on flexible substrate. *Jurnal Teknologi*, 75(7), 45-50.
22. Miandal, K.; Lam, M.L.; Shain, F.L.; Manie, A.; Mohamad, K.A.; and Alias, A. (2016). RF power dependence of ZnO thin film deposited by RF powered magnetron sputtering system. *Journal of Advanced Research in Materials Science*, 20(1), 6-13.
23. Mackenzie, R.C.I. (2016). *GPVDM user manual*, 38 pages.
24. Liu, C.H.; Yiu, W.C.; Au, F.C.K.; Ding, J.X.; Lee, C.S.; and Lee, S.T. (2003). Electrical properties of zinc oxide nanowires and intramolecular p-n junctions. *Applied Physics Letters*, 83(15), 3168-3170.
25. Keong, C.K.; Ahmad Hambali, N.A.M.; Wahid, M.H.A.; Ariffin, S.N.; and Shahimin, M.M. (2017). The optimal input voltage and emission rate characteristics for different LED chips material. *AIP Conference Proceedings*, 1835(1).
26. Jeon, H.; Ding, J.; Patterson, W.; Nurmikko, A.V.; Xie, W.; Grillo, D.C.; and Gunshor, R.L. (1991). Blue-green injection laser diodes in (Zn, Cd) Se/ZnSe quantum wells. *Applied Physics Letters*, 59(27), 3619-3621.
27. Nakamura, S.; Pearton, S.; and Fasol, G. (2001). *The blue laser diode: The complete story*. Heidelberg, Germany: Springer-Verlag Berlin Heidelberg.
28. Ryu, Y.R.; Kim, W.J.; and White, H.W. (2000). Fabrication of homostructural ZnO p-n junctions. *Journal of Crystal Growth*, 219(4), 419-422.